

Journal of Geophysical Research: Solid Earth

RESEARCH ARTICLE

10.1002/2017JB014425

Key Points:

- The kinematic vertical accelerations derived from carrier phase measurements are generally better than those from raw Doppler observations
- The accuracy of airborne gravimetry of GEOHALO experiment is about 1 mGal along the tracks from the crossover points
- Chekan-AM with the HALO jet can help to improve satellite-only gravity field models, especially in regions with sparse terrestrial data

Correspondence to:

B. Lu,
biaolu@gfz-potsdam.de

Citation:

Lu, B., Barthelmes, F., Petrovic, S., Forste, C., Flechtner, F., Luo, Z., He, K., & Li, M. (2017). Airborne gravimetry of GEOHALO mission: data processing and gravity field modeling. *Journal of Geophysical Research: Solid Earth Solid Earth*, 122. <https://doi.org/10.1002/2017JB014425>

Received 10 MAY 2017

Accepted 20 NOV 2017

Accepted article online 23 NOV 2017

Airborne Gravimetry of GEOHALO Mission: Data Processing and Gravity Field Modeling

Biao Lu^{1,2,3} , Franz Barthelmes² , Svetozar Petrovic² , Christoph Förste², Frank Flechtner^{2,3} , Zhicai Luo^{4,5}, Kaifei He⁶ , and Min Li^{2,3}

¹School of Geodesy and Geomatics, Wuhan University, Wuhan, China, ²GFZ German Research Centre for Geosciences, Potsdam, Germany, ³Department of Geodesy and Geoinformation Science, Technical University of Berlin, Berlin, Germany,

⁴MOE Key Laboratory of Fundamental Physical Quantities Measurement, School of Physics, Huazhong University of Science and Technology, Wuhan, China, ⁵Institute of Geophysics, Huazhong University of Science and Technology, Wuhan, China, ⁶School of Geosciences, China University of Petroleum, Qingdao, China

Abstract Airborne gravimetry is a crucial method to improve our knowledge about the Earth gravity field, especially in hard-to-access regions. Generally, the accuracy of airborne gravimetry is several milligals, which is suitable for filling the so-called polar gaps in satellite-derived global gravity field models. Here some investigations based on airborne gravity measurements from the GEOHALO mission over Italy are presented. To subtract the vertical accelerations from the values measured by the gravimeter, four different versions of kinematic accelerations were derived from Global Navigation Satellite Systems (GNSS) recordings. To remove the high-frequency noise, a low-pass filter with a cutoff wavelength of 200 s was applied to both Chekan-AM measurements and kinematic accelerations from GNSS. To investigate how future airborne gravity campaigns could be designed, a dedicated flight track was repeated two times showing that the equipment worked well also at higher altitude and speed. From the final best results follows an RMS of gravity differences at crossover points of 1.4 mGal, which, according to the law of error propagation, implies the accuracy of a single measurement to be $1.4/\sqrt{2} \approx 1$ mGal. To demonstrate how a satellite-only gravity field model can be improved by airborne measurements, a gravity field model for the GEOHALO region has been computed. To compute also an improved regional geoid model, the point mass modeling (PMM) and the remove-compute-restore (RCR) technique, using a recent satellite-only model and residual terrain modeling (RTM), were applied. Finally, GNSS/leveling points have been used to check the quality of the regional point mass model.

1. Introduction

The GEOHALO project includes different scientific experiments over Italy and adjacent regions over the Mediterranean: Global Navigation Satellite Systems (GNSS) navigation and positioning (He et al., 2016), GNSS reflectometry (Semmling et al., 2014), magnetometry, and laser altimetry (Scheinert, 2013). Airborne gravimetry is one of the main experiments of the GEOHALO project (Petrovic, Barthelmes, & Pflug, 2016). The characteristics of this mission were the following: total length of all profiles of about 16,150 km, an effective measurement time of approximately 33 h, mostly at an altitude of approximately 3,500 m, and an average speed of 425 km/h. Additionally, one ground track was repeated at a different altitude (10,500 m) and aircraft speed (720 km/h) which is also investigated in this paper to test the behavior of the equipment and to prepare for the planned future airborne gravity survey over Antarctica.

The High Altitude and LOng Range (HALO) aircraft (Figure 1, left) used in this experiment is a modified Gulfstream G550 business jet, which can reach altitudes of up to 15 km and has a long endurance of up to 10 h and a range of up to 4,000 km. This ensures that a gravimetry campaign can be also accomplished across hard-to-reach regions like mountains as well as the North and South Polar regions. Especially the latter is crucial because the most recent satellite-only gravity field models suffer from gaps over the polar regions which were caused by the inclination of the Gravity field and steady-state Ocean Circulation Explorer (GOCE) orbit of 96.7° (see, e.g., Lu, Luo, et al., 2017; Pail et al., 2011; Rudolph et al., 2002). Hence, the experiment described in this article is an airborne gravimetry study for exploring Antarctica in the future, too. The mobile airborne/marine gravimeter Chekan-AM used in this experiment was manufactured by CSRI Elektropribor



Figure 1. Equipments of airborne gravimetry of the GEOHALO mission: (left) the High Altitude and LOng Range (HALO) aircraft and (right) the Airborne/Marine Gravimeter Chekan-AM.

(Blazhnov, 2002). A picture of this gravimeter is given in Figure 1 (right). This kind of gravimeter has already been used on various airplanes and ships in many countries and there are consequently many operation experiences with this instrument (e.g., Krasnov, Sokolov, & Elinson, 2014; Krasnov, Sokolov, & Usov, 2011; Zheleznyak, 2010; Zheleznyak et al., 2015).

Any gravimeter, and hence also Chekan-AM, measures the total acceleration along the direction of the gravimeter sensitive axis which includes the gravity acceleration signal as well as all accelerations of the aircraft or ship. It turns out that even after filtering, the vertical accelerations of the aircraft strongly dominate the accelerations recorded by a gravimeter compared to the gravity variations along the trajectory. Hence, one of the main questions of airborne gravimetry is how to separate the vertical accelerations of the airplane (usually called kinematic accelerations) from the actual gravity accelerations which are both contained in the Chekan-AM measurements. The kinematic vertical accelerations are the first derivative of the kinematic vertical velocities, and the latter can be determined from GNSS measurements. Therefore, it is really important for airborne gravimetry in accurate GNSS processing to get highly accurate GNSS-derived kinematic accelerations. The first results of the GEOHALO campaign (Petrovic, Barthelmes, & Pflug, 2016, presented in 2013) were very preliminary and rather unsatisfactory. The main reason was that the GNSS-derived kinematic accelerations were not accurate enough. To improve the result, kinematic vertical accelerations derived from GNSS Doppler observations were included in the processing, and they are used for the airborne gravity data processing in this article as well.

The GNSS-derived kinematic velocities that are used to calculate the kinematic vertical accelerations can be based on two different kinds of Doppler observations (Cannon et al., 1997). One of them is the raw Doppler observations, and the other is derived from GNSS carrier phase measurements. Furthermore, GNSS velocity solutions can also be influenced by chosen sampling rates. In this study, we use 1 Hz and 10 Hz. We analyze these different GNSS velocity solutions and try to find out the best result for the airborne gravimetry of GEOHALO mission. For this, the gravity measurements along tracks derived at airplane altitude are compared with the corresponding values from a combined gravity field model. Additionally, the crossover points are analyzed to check the accuracy of the derived gravity measurements.

Subsequently, possible geodetic applications of this mission are studied. For example, a harmonic function based on the potentials of point masses was fitted to the airborne gravity measurements to show the extent of improvement with respect to a satellite-only gravity field model. Furthermore, a local quasi-geoid model has been calculated from the gravity measurements of this campaign. The method to build the local quasi-geoid is based on the combination of the point mass modeling and the remove-compute-restore (RCR) technique. In remove and restore steps, one calculated local quasi-geoid considers only the reference satellite-only gravity field model GO_CONS_GCF_2_DIR_R5 (DIR_R5) calculated by Bruinsma et al. (2014), while the other one considers the topography effects in addition. The main contents of this article are as follows: section 2 gives the basic processing strategy of airborne gravimetry of the GEOHALO mission, while section 3 gives the modeling methods for geodetic purposes of the airborne gravimetry measurements. Then section 4 demonstrates the numerical results and analysis. Finally, discussion and conclusions are presented in section 5.

2. Processing Strategy of Airborne Gravimetry

2.1. Processing of Gravimeter Recordings

The gravity sensor of Chekan-AM is designed as a double quartz elastic system (two quartz torsion fibers) to measure accelerations along the direction of the sensitive axis. This system is placed in a viscous liquid to damp high-frequency accelerations (vibrations). To keep the sensitive axis of this sensor in the vertical direction (precisely in the direction of the normal gravity), it is mounted on a GNSS-supported gyrostabilized platform (Sokolov, 2011). The equation for the calculation of the gravity value is

$$g = g_{\text{Chekan}} - a_{\text{GNSS}} + \delta g_{\text{Etv}} - \delta g_{\text{HAC}} - \delta g_{\text{drift}} + g_{\text{link}} \quad (1)$$

This is the fundamental equation of airborne and shipborne gravimetry, where g_{Chekan} is the raw gravity measurement from the Chekan-AM gravimeter. This raw gravity measurement is calculated from the position ($P(t)$) and velocity ($V(t)$) of the proof mass in the gravimeter as shown in equation (2). Here the acceleration information of the proof mass is ignored because of the strong damping by the liquid inside the gravimeter sensor unit:

$$g_{\text{raw}}(t) = C_1 \times P(t) + C_2 \times V(t) \quad (2)$$

C_1 and C_2 are constants for the respective gravimeter; t is the time of recording. The exact equation for the Chekan-AM gravimeter value is

$$\begin{aligned} g_{\text{Chekan}} = & b \times (m - m_0) + a \times (m - m_0)^2 \\ & + T_g \times \left(\frac{\partial(b \times (m - m_0) + a \times (m - m_0)^2)}{\partial t} \right) \end{aligned} \quad (3)$$

where b , m_0 , a , and T_g are constants determined during Chekan-AM's calibration; m is the sum of the recordings of the two sensors m_1 and m_2 . m_1 is calculated according to the equation

$$m_1 = \sum_{n=1}^N I_n n / \sum_{n=1}^N I_n \quad (4)$$

Here I_n is the intensity of pixel n ; n is the ordinal number of pixel, intensity of which in the code exceeds the specified level; and N is the number of pixels, intensity of which exceeds the specified level. This means that m_1 describes the position of the sensor, and equation (3) (which is a special case of equation (2)) is used to transform it into a measured acceleration. The m_2 reading is calculated similarly from the other quartz system.

Another main item in equation (1) is the GNSS-derived kinematic vertical acceleration of the moving platform a_{GNSS} . It is the first derivative of the kinematic velocity calculated from GNSS observations and explained in section 2.2.

Furthermore, δg_{Etv} is the *Eötvös* correction (Harlan, 1968; Jekeli, 2001). Here a slight smoothing by a moving-average filter is applied to the trajectory before computing the *Eötvös* correction to avoid systematic errors. δg_{drift} is the drift correction of the gravimeter which is calculated to be 1.88 mGal/d according to the known long time records (starts and ends of all flights) of the instrument during the GEOHALO campaign; g_{link} is the difference between the reference gravity value and the measurement of Chekan-AM at the base station; δg_{HAC} is the horizontal acceleration correction as the vertical acceleration is also influenced by horizontal components. It is also called Harrison effect (LaCoste, 1967; Swain, 1996). Generally, the correction for the Harrison effect is calculated according to the instructions from the manufacturer of the gravimetry equipment (Krasnov & Sokolov, 2015). From our investigation, in the GEOHALO mission the RMS value of the Harrison effect after filtering is 0.45 mGal. Furthermore, the RMS of absolute differences at crossover points is 1.50 mGal without taking this correction into account (L1 (1 Hz)a), while it is 1.39 mGal with this correction included (L1 (1 Hz)), as shown in Table 2. The Harrison effect is small and only up to 1 mGal in a few situations, but it should be taken into account with an accuracy goal of 1 mGal or better.

2.2. Determining the Kinematic Trajectories and Accelerations From GNSS

The GNSS kinematic trajectories are based on multiple reference stations and multiple kinematic stations (two) as shown by He et al. (2016). From the results, this method can effectively improve the reliability and accuracy of the kinematic relative positioning down to 1–2 cm accuracy. With respect to the aim to reach an

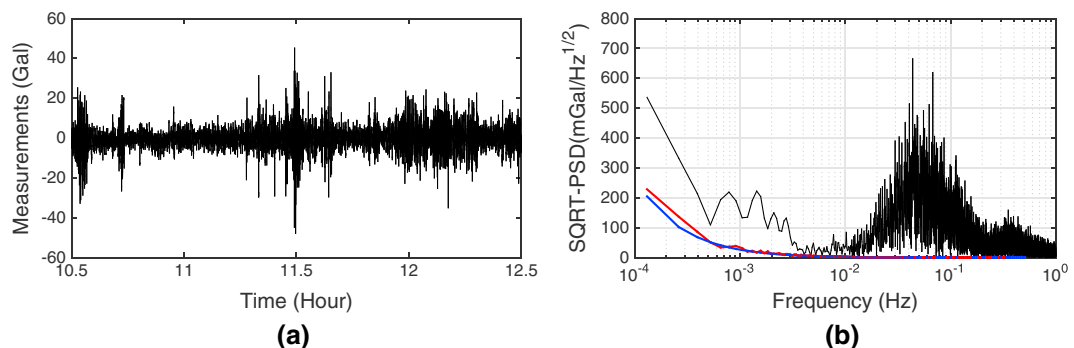


Figure 2. (a) Unfiltered measurements, and (b) their spectral densities (the black line), of the gravimeter along a typical track of the GEOHALO mission. The blue line in Figure 2b represents the spectral densities of “real” gravity calculated from gravity field model EIGEN-6C4; the red line in Figure 2b represents the spectral densities of the final gravimetry measurements after filtering.

accuracy of 1 mGal or better for the airborne gravity measurements, the horizontal accuracy of the position is not critical because the gravity field does not change much if we change the horizontal position. In contrast, the accuracy of the vertical component of the position must be much better since the vertical gravity gradient is about 0.3086 mGal/m. Hence, the positioning accuracy of 1–2 cm is sufficient for airborne gravimetry. So the main problem is to determine the kinematic velocities of the platform which are used to calculate the kinematic vertical accelerations by computing the vertical derivatives using cubic spline interpolation.

Two methods are used in this study to determine the velocity of the aircraft from GNSS (see He, 2015). One is based on raw Doppler observations (Borio et al., 2009; Cannon et al., 1997; Szarmes et al., 1997). This method is theoretically rigorous and dependent on the accuracy of raw Doppler observations. The kinematic velocity from raw Doppler observations of higher sampling rates (10 Hz) may provide us more accurate acceleration information compared to that of lower sampling rates (1 Hz). The other method is also based on Doppler observations which are, in contrast, derived from carrier phase measurements (Bruton et al., 1999; Cannon et al., 1997; Serrano et al., 2004). The accuracy of carrier phase observations is higher than of raw Doppler observations. However, the second method needs to incorporate cycle slip detection and correction. The velocity determination for the aircraft in the second method is additionally influenced by the movement state of the aircraft. One assumption here is that the carrier phase variation rate obtained by differencing between epochs represents the instantaneous variation rate with the time. From this point of view, we should record measurements of a sampling rate as high as possible. But in reality, the noise of the carrier phase variation rate will be enlarged as the sampling rate is increased. Therefore, we use both methods to calculate kinematic velocities with two different sampling rates (1 Hz and 10 Hz) and investigate which gives the best result.

One problem is that the raw accuracy of various kinematic vertical acceleration estimation approaches cannot meet the requirements of airborne (several milligals or even better) and shipborne (submilligal) gravimetry. Fortunately, the noise of the kinematic vertical accelerations derived from the kinematic velocities of the aircraft mainly affects the high frequencies. Therefore, we analyze the different results after applying a low-pass filter.

2.3. The FFT Low-Pass Filter

Although we expect gravity variations of several tens of milligals up to a maximum of 100 or 200 mGal in the Mediterranean area, the range of the measurements recorded by the Chekan-AM gravimeter spans over several 10,000 mGal for a typical track of the GEOHALO mission (see Figure 2a). The reason is the kinematic vertical accelerations of the aircraft (which are, of course, inherent in the measurements of the gravimeter), possible influences of these accelerations onto the gravimeter which could cause additional errors, and other corrections in equation (1). Fortunately, as can be seen in Figure 2b, most of the power is concentrated in the high-frequency part which cannot be generated by the variation of the “real” gravity field along the track (the blue line in Figure 2b is calculated from gravity field model EIGEN-6C4 Förste et al., 2014). Therefore, it is obvious that the high-frequency part can easily be filtered out by applying an appropriate low-pass filter (the red line in Figure 2b represents the final gravimetry measurements after filtering). For this low-pass filtering we used the technique of fast Fourier transformation (FFT) (Cooley & Tukey, 1965). The data to be filtered

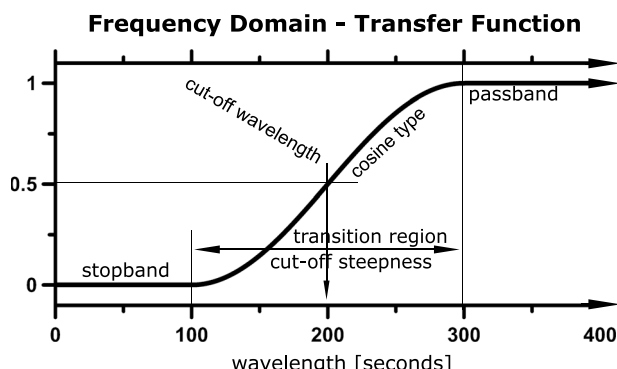


Figure 3. Transfer function of the low-pass filter to be applied in the frequency domain.

are transformed by FFT into the frequency domain and multiplied by a specific transfer function. Finally they are retransformed back into the time domain by inverse FFT. This technique has been described for airborne gravimetry by Childers, Bell, and Brozena (1999). In our processing, a window with cosine type at both edges (Tukey window) is applied to the measurements before the FFT low-pass filtering to avoid sudden jumps at the beginning and end of the data sets. It should be noted that this approach is not suitable for real-time processing, but it does not produce any phase shift compared to the widely used low-pass filtering in airborne gravimetry like Butterworth filter in the time domain. A further advantage is that the filter which is characterized by cutoff wavelength, transition range (sharpness or steepness of cutoff), and the shape of the transfer function can be simply defined directly in the frequency domain as shown in Figure 3.

3. Modeling of Gravity Disturbance and of the Quasi-Geoid

After having processed the GEOHALO airborne gravimetry measurements, geodetic applications were performed to demonstrate the usefulness of this experiment. Although the global models like EIGEN-6C4 are already very good and have a spatial resolution of about 10 km over the region of this mission (see also Barzaghi et al., 2016), we wanted to investigate the situation for a region where the gravity field is based on satellite measurements only. Hence, we want to know how a satellite-only model can be improved regionally by using only the airborne measurements and available topography information and, in particular, how good a derived regional quasi-geoid can be.

To compute a gravimetric quasi-geoid, a harmonic function has to be fitted to the gravity measurements which then can be used to compute the quasi-geoid. Strictly, the computation of a geoid from gravity measurements is only possible globally. Therefore, to reduce the influence of the gravity field outside the surveyed area, a satellite-only model containing the long-wavelength part of the gravity field is subtracted beforehand (and readded afterward). The result is a regional gravity field model (i.e., also a geoid) with the resolution of the airborne measurements. To improve this resolution, the available information of the highly resolved topography can be used additionally.

To model the gravity field regionally or locally, spherical radial basis functions are widely used and investigated (see, e.g., Klees et al., 2008; Wittwer, 2009; Wu et al., 2017). Point mass potentials are the most simple and natural radial basis functions (see, e.g., Barthelmes, 1986, 1988; Barthelmes & Dietrich, 1991; Claessens, Featherstone, & Barthelmes, 2001), and we use this method to fit the gravity disturbances to model the regional gravity field and, hence, the quasi-geoid.

3.1. Modeling Method

According to Newton's law of gravitation (see Newton et al., 1833), the equation for the potential generated by one point mass is

$$\phi = \frac{Gm}{l} \quad (5)$$

and the gradient of this potential, that is, the vector of the gravitational acceleration related to the potential of a point mass, is

$$\text{grad } \phi = \frac{Gm}{l^2} \vec{l} \quad (6)$$

where G is the Newtonian gravitational constant, m is the magnitude of the point mass, l and \vec{l} are distance and distance vector between the computation point and the point mass, respectively. As mentioned before, the long-wavelength part is subtracted prior to the fit of the point masses. Here two options are applied: (1) subtraction of the normal gravity γ_{wgs84} related to the ellipsoidal normal potential U_{wgs84} of the reference system WGS84 and (2) subtraction of the gravity g_{satmodel} related to the potential W_{satmodel} of a satellite-only model. The gravity disturbance in point P is defined as

$$\delta g = g(P) - \gamma(P) \quad (7)$$

where g is the measured gravity related to the potential W , and γ can be (1) $\gamma = \gamma_{\text{wgs84}}$ or (2) $\gamma = g_{\text{satmodel}}$. These two types of gravity disturbances have to be approximated by a point mass model. Hence, we have to model the two different disturbance potentials: $T = W - U_{\text{wgs84}}$ and $T = W - W_{\text{satmodel}}$. If the disturbing potential and its gradient are modeled by N point masses m_i at the positions q_i , we get

$$\begin{aligned} T(P) &= \sum_{i=1}^N \frac{Gm_i}{l(P, q_i)} \\ \vec{\delta}g(P) = \text{grad } T(P) &= \sum_{i=1}^N \frac{Gm_i}{l^2(P, q_i)} \frac{\vec{l}(P, q_i)}{l(P, q_i)} \\ \delta g(P) &\approx \sum_{i=1}^N \frac{Gm_i}{l^2(P, q_i)} \left(\frac{\vec{\gamma}_{\text{wgs84}}}{\gamma_{\text{wgs84}}} \cdot \frac{\vec{l}(P, q_i)}{l(P, q_i)} \right) \end{aligned} \quad (8)$$

where $l(P, q_i)$ is the distance between the mass point (q_i) and the computation point (P). The gravity disturbance δg is not the magnitude of the gravity disturbance vector $\vec{\delta}g$ but the difference of the magnitudes of g and γ (see formula (7)), which can be approximated by projecting the vector $\vec{\delta}g$ onto the direction of the normal gravity $\vec{\gamma}/\gamma$. In this article, the point mass method is used with fixed positions for the masses and the masses are the free parameters to be fitted. To avoid contributions of the point mass model in areas without measurements, the masses are distributed only below measurements. Although the resolution of airborne gravity measurements is about 12 km along the tracks, the distance between the tracks is about 40 km. Therefore, the masses are distributed below the tracks also with a 40 km spacing to ensure an isotropic spatial resolution. There are different criteria to define the depth of masses. One is the best r formula by Hardy and Göpfert (1975) which delivers a depth of approximately 23 km for a horizontal distance of 40 km. This means that the depth should not be less than 23 km. If masses are situated too shallow (e.g., at depths much less than the horizontal distance), the approximation in areas between the masses would be wrong. If the depth is too big, the computation of the masses would be unstable. So we found that a depth of 40 km is a good compromise between the smoothness of the point mass model and a stable solution.

The point mass method is used in three different schemes. First, the masses are fitted to the gravity disturbances $g - \gamma_{\text{wgs84}}$ (at flight altitude) to compare the result with a combined gravity field model of the same resolution to check the method. Second, the masses are fitted to the gravity disturbances $g - g_{\text{satmodel}}$ (at flight altitude) and the result is used to compute the quasi-geoid (height anomaly ζ) by Bruns' formula $\zeta = T/\gamma$. Third, the topography effects are considered additionally during the RCR computation. Residual terrain modeling (RTM) reduction is used to calculate topography effects in this research and will be explained in detail in the next subsection. Furthermore, besides the comparison with a good global model, GNSS/leveling points within the local area are used to check the quality of the quasi-geoid.

3.2. RTM Reduction

RTM reduction was introduced by Forsberg (1984) based on a smooth mean elevation surface, which is usually derived by applying a moving-average filter to the existing high-resolution Digital Terrain Model (DTM) model (Dahl & Forsberg, 1998; Denker, 2013) or a high-order spherical harmonic expansion of the topography of the Earth (Hirt, 2013), for example, RET2012. In order to calculate RTM effects from the residual topography, the tesseroid approach is chosen in our research. Compared to the formulas of RTM effects derived by using rectangular prisms, tesseroids offer a better approximation of the Earth surface as no gaps exist between the neighboring tesseroids, no coordinate system transformation is needed, and the computation time is decreased as shown by Heck and Seitz (2007). The basic formula for the RTM effect (the gravitational potential v), derived from a spherical tesseroid of homogeneous mass-density ρ , is

$$v(r, \varphi, \lambda) = G\rho \int_{\lambda_1}^{\lambda_2} \int_{\varphi_1}^{\varphi_2} \int_{r_1}^{r_2} \frac{r'^2 \cos \varphi' dr' d\varphi' d\lambda'}{l} \quad (9)$$

where $l = \sqrt{r^2 + r'^2 - 2rr' \cos \Psi}$ means the distance between the computation point $P(r, \varphi, \lambda)$ and the running integration point $Q(r', \varphi', \lambda')$, $\cos \Psi = \sin \varphi \sin \varphi' + \cos \varphi \cos \varphi' \cos(\lambda - \lambda')$. The gravitational effect is the derivative of v with respect to r . More details concerning the formulas for the RTM reduction are given by Heck and Seitz (2007). The advantage of the RTM reduction is that the influence of the distant topographic masses cancels out due to the oscillation of the density anomaly between positive and negative values. Thus,

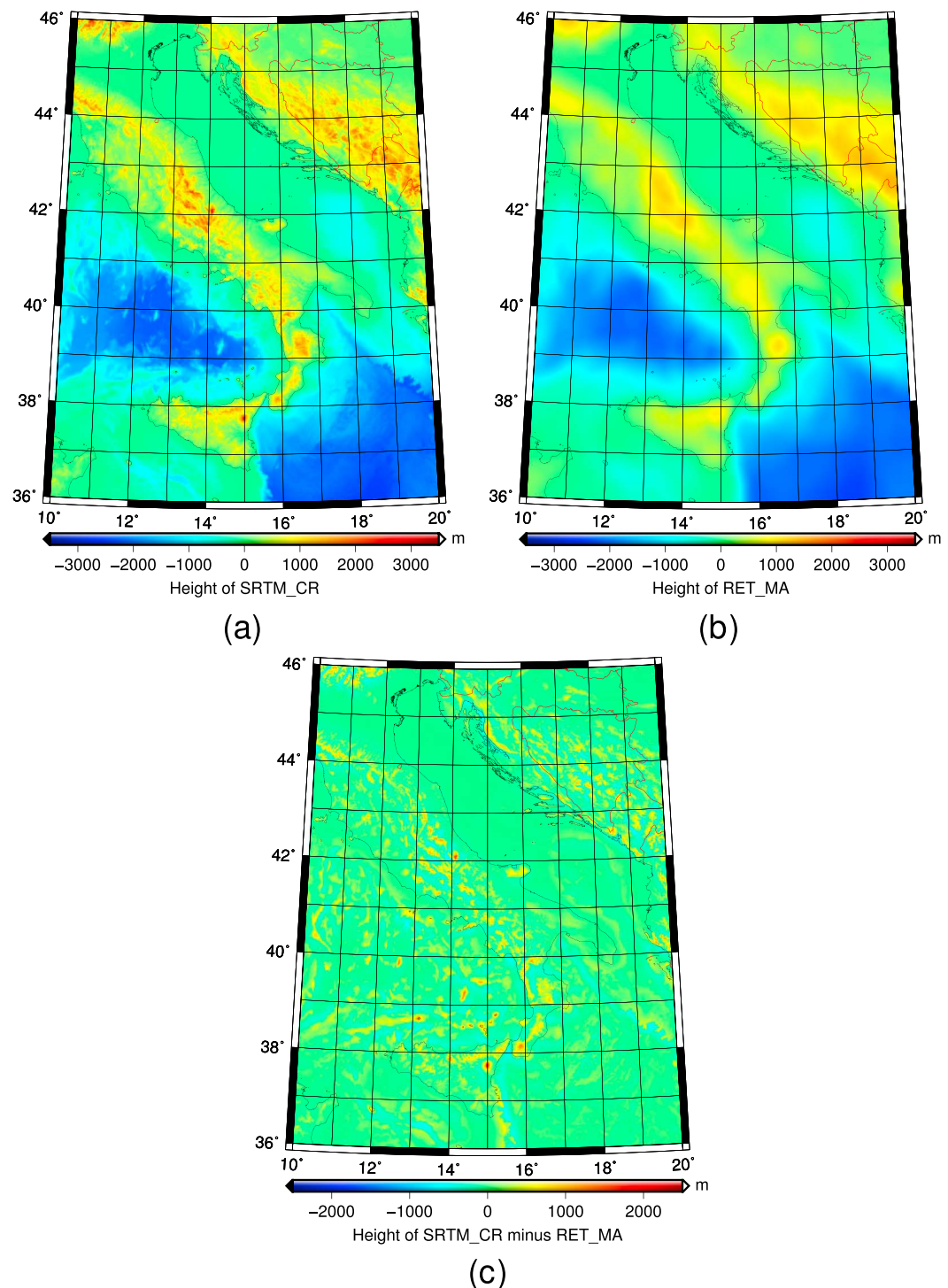


Figure 4. Topography: (a) SRTM_CR surface, (b) RET_MA surface, and (c) the residual surface SRTM_CR minus RET_MA.

the integration for computing RTM corrections could be done in a limited region only instead of a global integration. Moreover, the RTM reduction gives similar results as topographic-isostatic reduction which smooths the regional gravity field significantly at very short scales and introduces no large long-wavelength aliasing errors as shown by Forsberg (1984).

In this article, SRTM_CR (combined and rock-equivalent over the oceans) is used as the high-resolution digital topographic elevation, while RET_MA is the smooth mean elevation surface derived by applying a

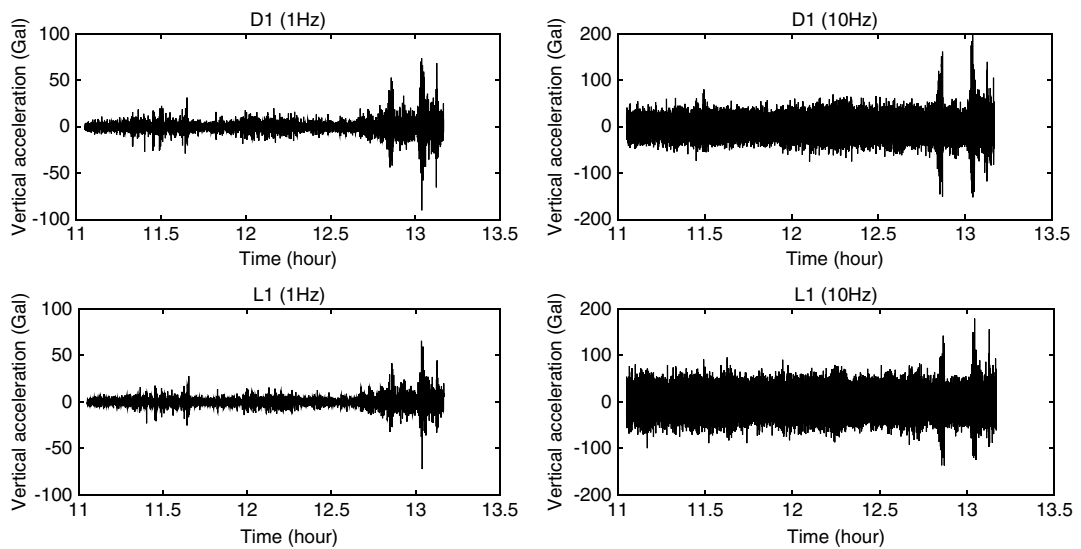


Figure 5. Vertical accelerations from different Doppler observations (D1 = raw Doppler data, L1 = carrier phase-derived Doppler data) and two sampling rates for track R11-12 before filtering.

moving-average filter to SRTM_CR. In detail, SRTM_CR is derived in two steps. First, the 3 arc sec SRTM V4.1 model is merged with 15 arc sec SRTM15_PLUS model. SRTM15_PLUS is interpolated to 3 arc sec before inserting the SRTM15_PLUS bathymetric depths into the V4.1 release over ocean areas. In the second step, the rock-equivalent topography (RET) approach is applied to reduce the ocean depths by a factor of 0.614 to equivalent rock heights as proposed by Hirt (2012, 2013) and Rummel et al. (1988). The use of RET is convenient due to a single constant uniform mass-density of $2,670 \text{ kg/m}^{-3}$ for the RTM reduction. Lastly, the relevant topography data (SRTM_CR, RET_MA, and residual SRTM_CR minus RET_MA) are shown in Figure 4.

4. Numerical Results and Analysis

4.1. Gravimetry Results of GEOHALO Mission

The two different kinds of GNSS-derived kinematic velocities with two different sampling rates are calculated to derive kinematic vertical accelerations, based on raw Doppler observations at 1 Hz and 10 Hz as well as on Doppler observations derived from carrier phase measurements at 1 Hz and 10 Hz. We try to find the best result by two criteria. The first criterion is to compare the airborne gravity results with the Earth gravity field model EIGEN-6C4, because it is accurate in this area based on good and dense terrestrial gravimetric data.

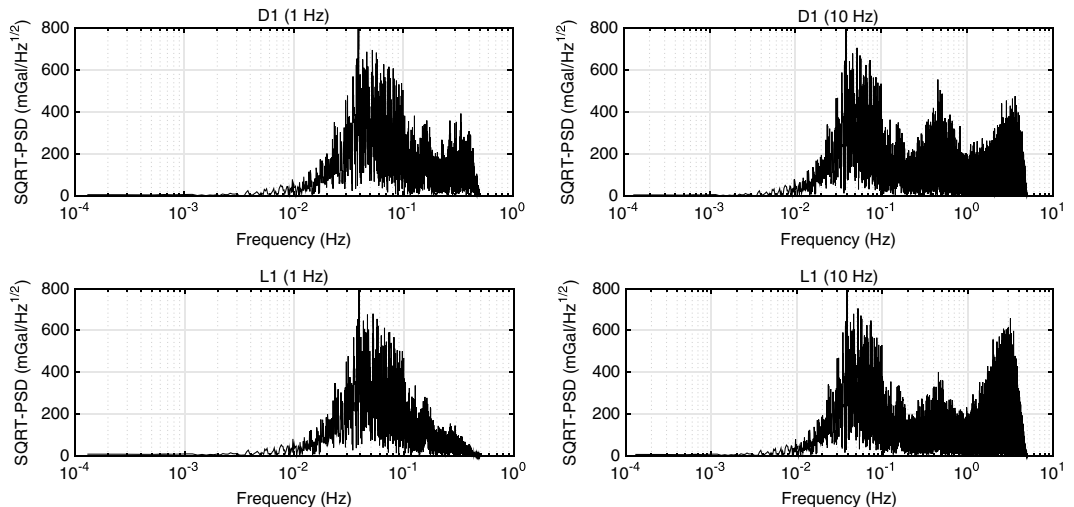


Figure 6. Spectral densities for vertical accelerations from different Doppler observations (D1 = raw Doppler data, L1 = carrier phase-derived Doppler data) and two sampling rates for track R11-12 before filtering.

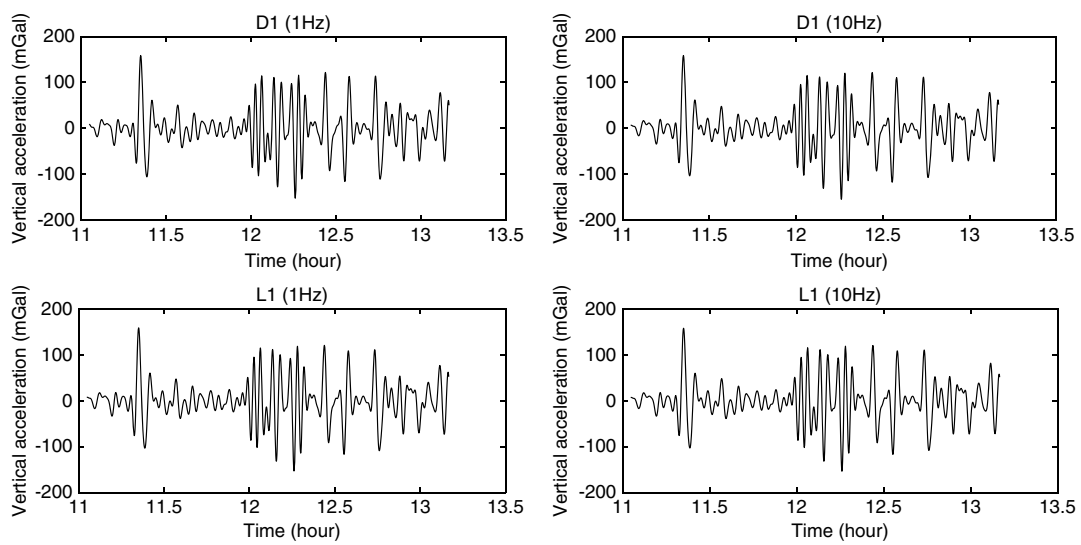


Figure 7. Vertical accelerations from different Doppler observations (D1 = raw Doppler data, L1 = carrier phase-derived Doppler data) and two sampling rates for track R11-12 after filtering.

The cutoff wavelength of the low-pass filter is 200 s. As the velocity of the aircraft is about 120 m/s, the half wavelength in a spatial resolution is about 12 km along the tracks, which corresponds to the resolution of EIGEN-6C4. Another criterion is to check the differences at crossover points.

First, for the track named R11-12 the GNSS-derived kinematic vertical accelerations from different methods and sampling rates are shown. Figure 5 displays the four different GNSS-derived kinematic vertical accelerations before filtering: D1 (1 Hz) and D1 (10 Hz) are the results from raw Doppler observations for 1 Hz and 10 Hz sampling rates, respectively; L1 (1 Hz) and L1 (10 Hz) mean the 1 Hz and 10 Hz results from Doppler observations derived from carrier phase measurements, respectively. In this figure, the high sampling rate accelerations are larger than the low sampling rate accelerations. There is large noise in the high-frequency part which can be seen from the spectral densities shown in Figure 6. By comparing the different spectral results in Figure 6, the high-frequency noise is larger for the high sampling rate results than for the low sampling rate. Therefore, a low-pass filter should necessarily be applied to check the results. After filtering, as shown in Figure 7, the GNSS-derived kinematic vertical accelerations are mutually similar. The differences between these vertical accelerations are shown in Figure 8: D1 (10 Hz), L1 (1 Hz), and L1 (10 Hz) are close to

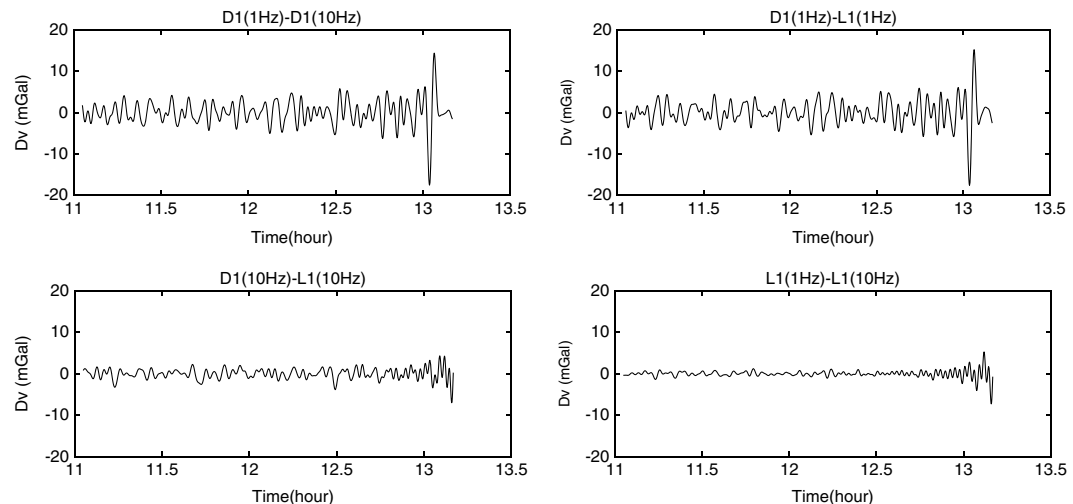


Figure 8. Differences between vertical accelerations from different Doppler observations (D1 = raw Doppler data, L1 = carrier phase-derived Doppler data) and two sampling rates for track R11-12 after filtering.

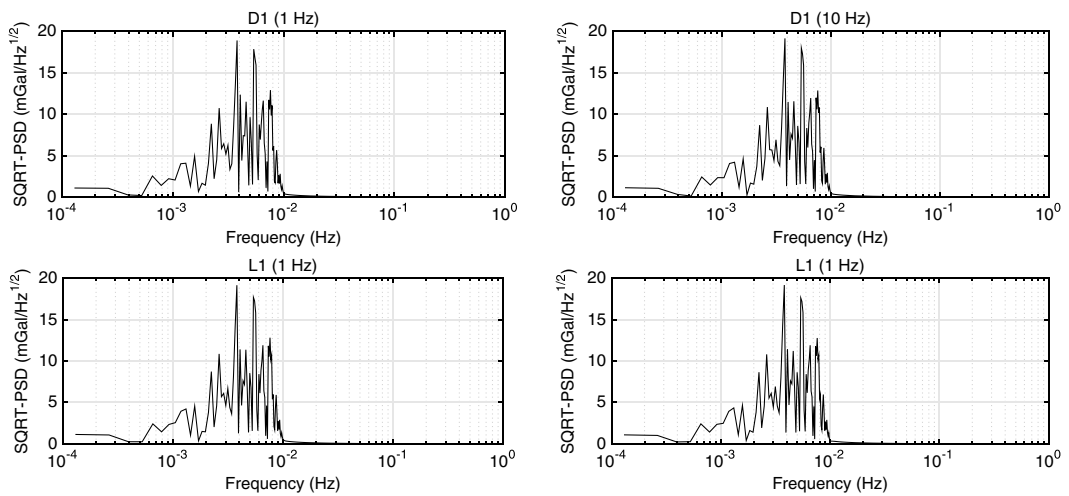


Figure 9. Spectral densities for vertical acceleration from different Doppler observations (D1 = raw Doppler data, L1 = carrier phase-derived Doppler data) and two sampling rates for track R11-12 after filtering.

each other, but the differences from D1 (1 Hz) are somewhat larger. Figure 9 shows the spectral densities for vertical accelerations after filtering, and the differences among these four different accelerations are shown in Figure 10. The spectral differences are very small among D1 (10 Hz), L1 (1 Hz), and L1 (10 Hz) but a little larger to D1 (1 Hz). The differences obtained using all tracks together are given later on in the frame of the comparisons based on the two criteria mentioned before, which are used to find the best result.

Table 1 shows the statistics of gravity differences between our airborne gravity data and gravity values derived from EIGEN-6C4. It can be seen that the result obtained using L1(10 Hz) is closest to EIGEN-6C4, and its RMS is 2.85 mGal. The result based on Doppler observations derived from GNSS carrier phase measurements is a little more accurate than the result based on GNSS raw Doppler observations. However, the result from D1 (10 Hz) is very close to L1 (1 Hz) and L1 (10 Hz), which means that the high sampling rate raw Doppler observations are useful to calculate the velocity and acceleration of the platform. From the third column of this table, it follows that the mean values of differences from these four different results are almost the same, which means that there may exist a constant bias of about -0.89 mGal.

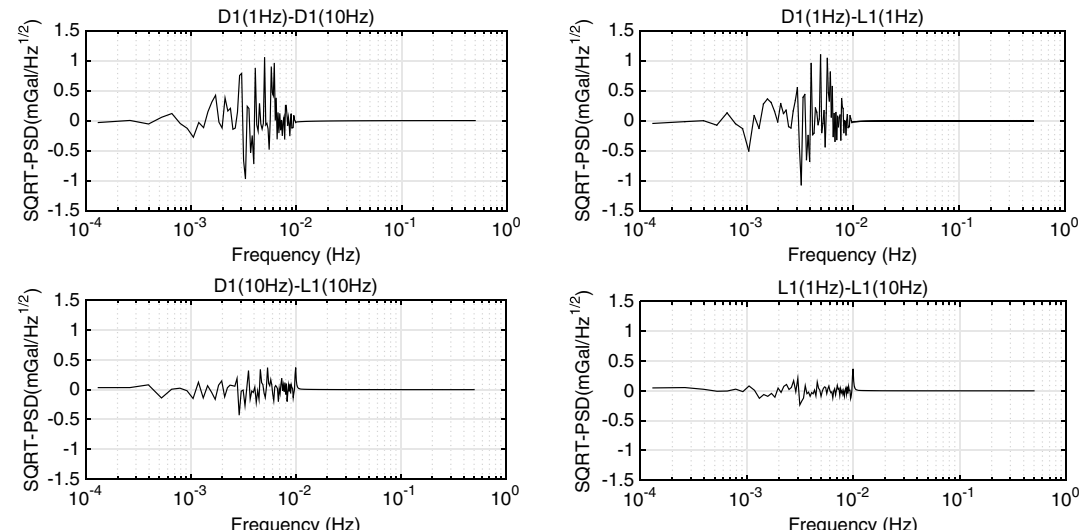


Figure 10. Differences between spectral densities for vertical acceleration from different Doppler observations (D1 = raw Doppler data, L1 = carrier phase-derived Doppler data) and two sampling rates for track R11-12 after filtering.

Table 1

Statistics of Gravity Differences Between Airborne Gravity Results (70,760 Points) and Gravity Values Derived From EIGEN-6C4

	Minimum	Maximum	Mean	RMS
D1(1 Hz)	-29.32	23.01	-0.89	4.17
D1(10 Hz)	-16.46	16.45	-0.89	2.97
L1(1 Hz)	-16.29	16.29	-0.89	2.88
L1(10 Hz)	-15.76	15.79	-0.89	2.85

Note. Unit: mGal.

Table 2 gives the statistics of absolute gravity differences at crossover points. Their positions are shown in Figure 11a. The total number of crossover points is 20, but we only use 17 of them (colored green) because two crossover points (in red) are obviously outliers which are near ends of the tracks. The third unused crossover point (in black) is also an outlier because there is a jump (of about 5 mGal) in one track which obviously comes from turbulences and could not be reduced by the GNSS-derived kinematic accelerations. It can be seen from the table that the results from Doppler observations derived from carrier phase measurements are better than those from raw Doppler observations. By comparing the 1 Hz and 10 Hz results of L1, the RMS of L1(1 Hz) is 1.39 mGal, which is better than L1(10 Hz) of 1.54 mGal.

By analyzing the results from these two criteria, it seems that the kinematic velocity determined from Doppler observations derived from carrier phase measurements is more accurate than that from raw Doppler observations. Furthermore, the sampling rates of 1 Hz and 10 Hz are both useful and the differences of the final results from these two different sampling rates are very small. The final accuracy of 1–2 mGal from crossover points is acceptable. On the other hand, the accuracy of the comparison with EIGEN-6C4 is about 3 mGal, which means that airborne gravimetry can improve the current model at locations with lack of good quality gravimetry data, such as Antarctica. Here, the best airborne gravimetry data from the GEOHALO project can be found from GFZ Data Service (Lu, Barthelmes, et al., 2017).

Since it was a test campaign, a “repeat track” was flown two times over almost the same ground track but at two different altitudes. The positions of the overlaid two tracks are shown in Figure 11b. Track R11-12 (red) had an average height of 3,577.8 m, and H03-02 (yellow) was flown at an average height of 10,490.4 m. Another difference between these two tracks is the speed of the aircraft. The mean speed of the aircraft at the lower track was about 425 km/h but approximately 720 km/h at the higher one. The gravity disturbances along these two tracks and the differences between the airborne gravimetry results and EIGEN-6C4 are studied; to compare these two tracks, see Figure 12. It can be seen that the gravity disturbance differences of these two tracks look reasonable: The gravity disturbances of track H03-02 (with higher speed and altitude) are smoother than those of track R11-12 (with lower speed and altitude). The oscillations of the gravity disturbances at 10,000 m are smaller and smoother due to a strong damping of the shorter wavelengths of the gravity field with increasing altitude (see Figure 12). The RMS of the differences between the gravity disturbances based on the Chekan-AM measurements and those derived from EIGEN-6C4 for these two tracks are 3.24 mGal and 3.08 mGal, respectively. According to potential theory it is not strictly possible to upward (or downward)

Table 2

Statistics of Absolute Differences at Crossover Points

	Minimum	Maximum	Mean	RMS
D1(1 Hz)	0.20	4.03	2.08	2.47
D1(10 Hz)	0.20	3.26	1.68	1.87
L1(1 Hz)	0.12	2.52	1.22	1.39
L1(1 Hz)a	0.24	2.42	1.33	1.50
L1(10 Hz)	0.01	3.34	1.22	1.54

Note. Unit: mGal. L1(1 Hz)a is without the horizontal accelerations correction, while others are with this correction.

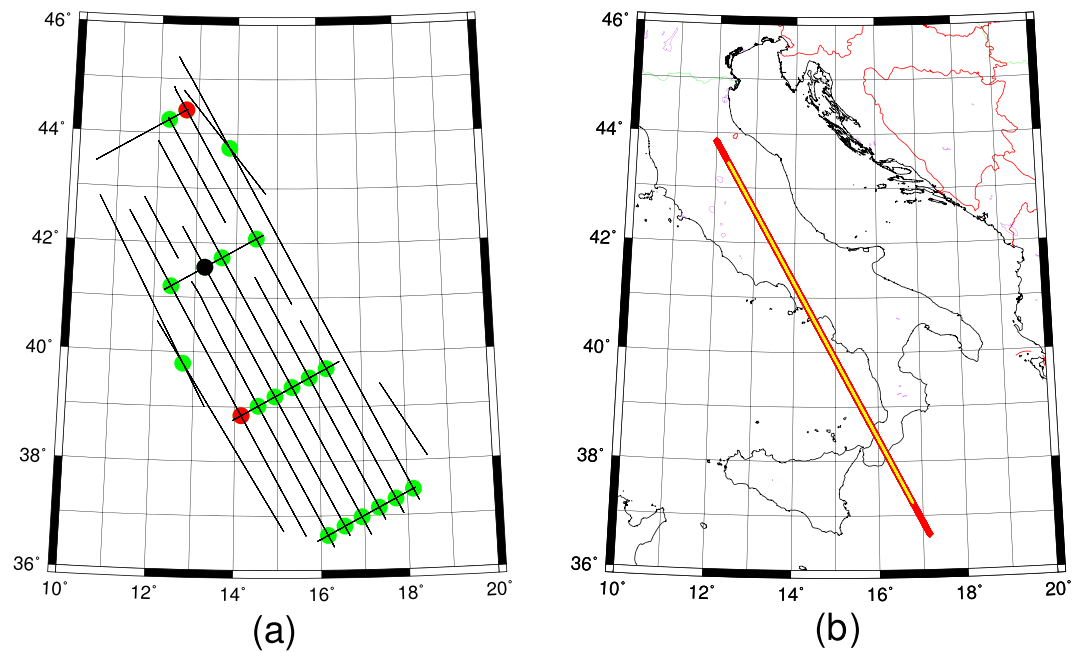


Figure 11. (a) Tracks and crossover points: two red crossover points and one black crossover point are outliers and (b) Repeat tracks: H03-02 and R11-12 with average altitude of 10,490.4 m (yellow) and 3,577.8 m (red), respectively.

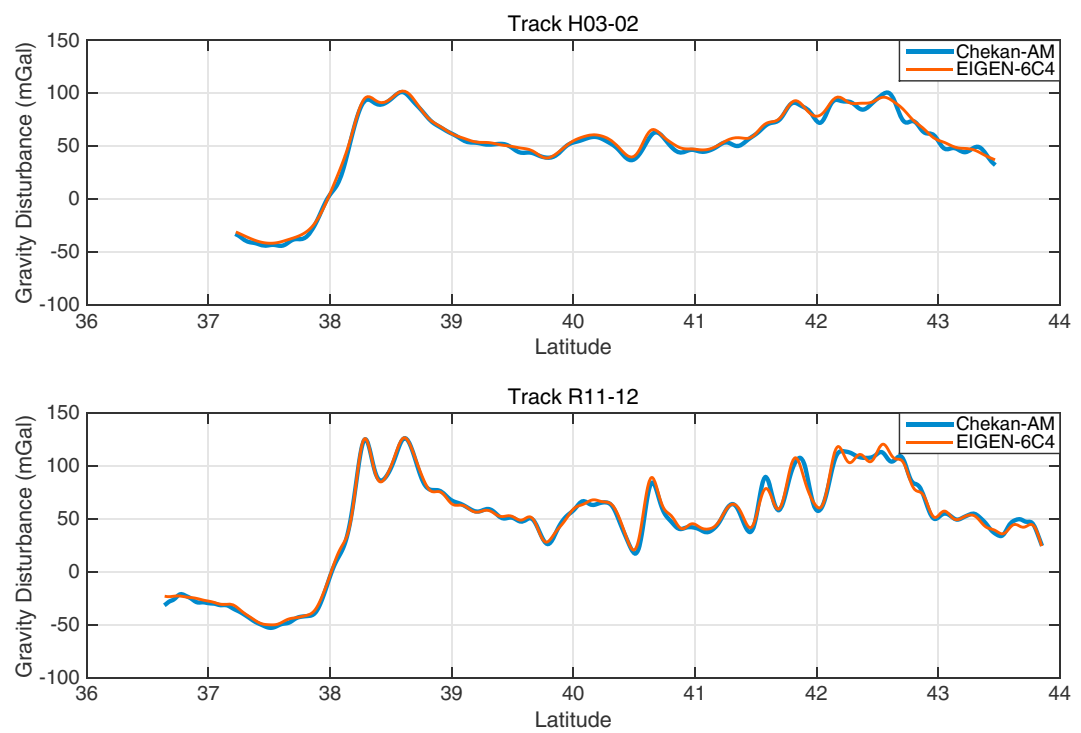


Figure 12. Gravity disturbances at flight altitude of the repeat tracks (H03-02 and R11-12) compared with those derived from EIGEN-6C4.

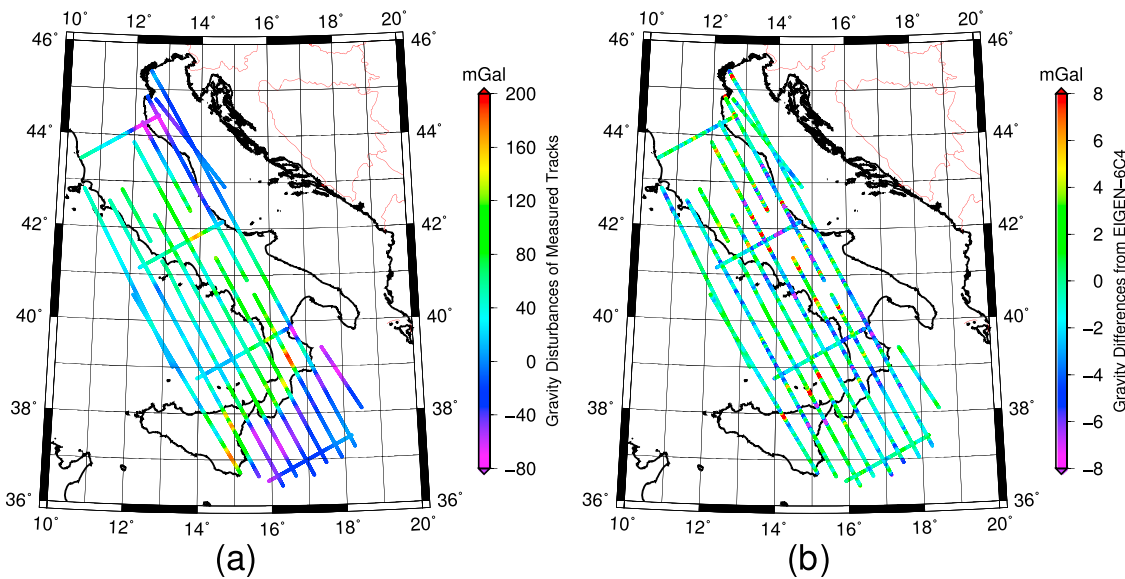


Figure 13. (a) Measured gravity minus the normal gravity of WGS84 and (b) gravity differences between Chekan-AM's measurements and that from EIGEN-6C4 (degree/order (d/o) 2190).

continue gravity measurements along an individual track without knowing the real three-dimensional gravity field. Nevertheless, we do it approximately to compare these two tracks. A low-pass filter with a longer cutoff wavelength (340 s) is applied to the low track R11-12 which gives approximately the same spatial resolution (≈ 20 km) as the high track H03-02 (which was flown with higher speed). Then, the low track R11-12 is upward continued using the difference of the gravity field model EIGEN-6C4 at the two altitudes. The RMS of gravity differences between these two tracks after upward continuation is 4.40 mGal. The applied upward continuation contains some approximations; for example, the “real” gravity gradient comes from the gravity model and the spatial resolutions of these two tracks are not exactly the same due to the different aircraft velocities and different low-pass filter parameters.

Figure 13a shows gravity disturbances along all tracks. They range from -80 to 200 mGal. From this figure, it is obvious that the gravity disturbances are large over the Italian part of the European continent and small over the Mediterranean sea. Further, Figure 13b shows gravity differences between the Chekan-AM measurements and EIGEN-6C4. Again, it can be seen that the differences are mainly large over the continent and small over the sea. As already mentioned, airborne gravity measurements are expected to be more accurate than the gravity field model EIGEN-6C4, especially over land. The Italian ground gravity coverage is quite poor in the Alpine region and some areas of the Apennines. In addition, the comparison between preliminary GEOHALO gravimetry measurements (which are low accurate with low resolution) and Italian ground-based data has shown that there exist some biased ground data in the northern area of the Adriatic Sea (Barzaghi et al., 2016). Therefore, the latest processed airborne gravimetry measurements of GEOHALO mission in this article are expected to further assess the quality and homogeneity of the Italian ground-based data.

4.2. Gravimetric Geoid

To investigate how well a geoid (quasi-geoid) can be derived on the basis of the gravity measurements of the GEOHALO mission, a point mass model is fitted to the measurements. The corresponding spatial resolution of 40 km corresponds to maximum degree and order of approximately 500 of a global model in terms of spherical harmonics, which means that airborne gravimetry on board the HALO aircraft has the potential to improve a satellite-only gravity field model of such maximum degree and order. The plots in Figure 14 show a comparison between the gravity disturbances modeled from our airborne measurements and derived from the combined global model EIGEN-6C4 truncated at degree 500. The areas with larger differences (Figure 14c) lie mainly at the borders and in areas without GEOHALO measurements, that is, without point masses (see Figure 14b) and can thus be explained. The reasons for the remaining differences could be, obviously, errors in

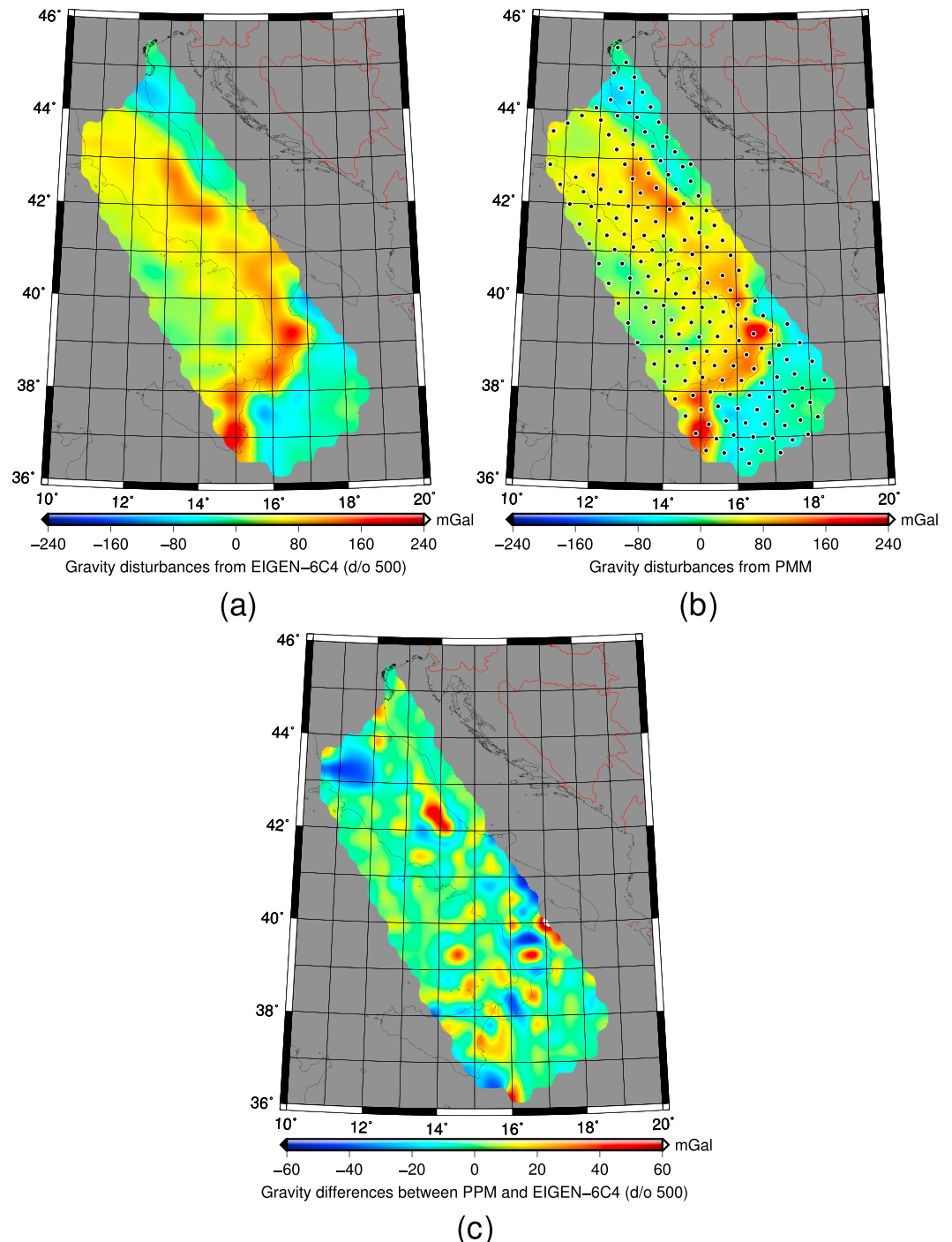


Figure 14. (a) Gravity disturbances on the ellipsoid of the model EIGEN-6C4 up to $N_{\max} = 500$, which is the resolution expected due to the 40 km track distance, (b) gravity disturbances on the ellipsoid of the point mass model (183 masses) computed alone from the airborne gravity values at flight altitude, and (c) gravity differences between these two models (the point mass model (183 masses) minus EIGEN-6C4 (d/o 500)) on the ellipsoid.

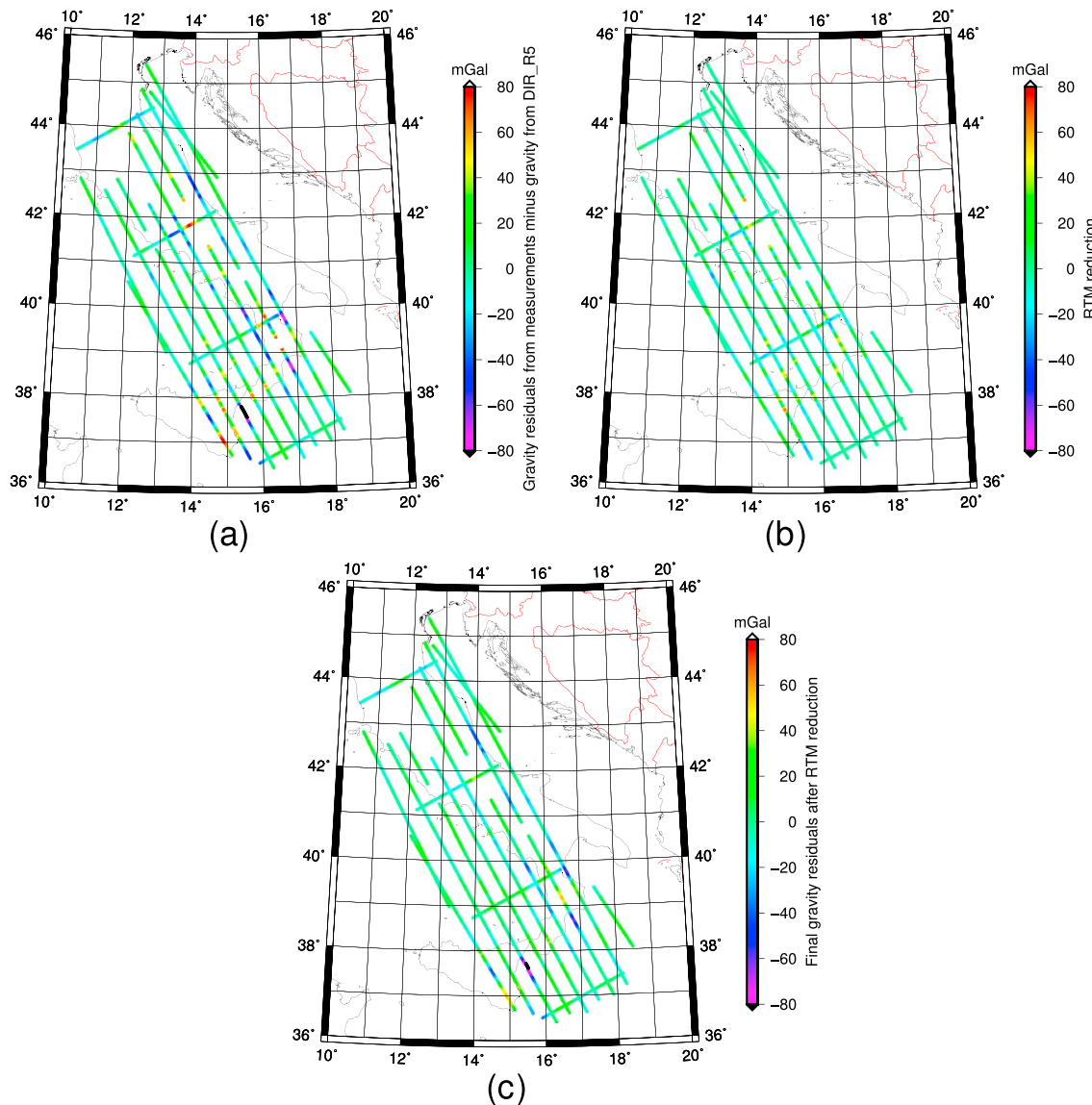


Figure 15. (a) Measured gravity minus the satellite-only model DIR_R5, (b) gravity values calculated from RTM reduction and, (c) measured gravity minus the satellite-only model and RTM reduction.

(at least) one of the models. A further aspect is that we compare two models with different mathematical basis functions. This means that the truncated spherical harmonic model does not contain wavelengths shorter than those related to degree 500, whereas although the spherical harmonic spectrum of the point mass model decays rapidly after degree 500 due to the depth of 40 km, nevertheless, shorter wavelengths are still in the model.

Furthermore, the local quasi-geoid is calculated without and with RTM reduction. Figure 15a shows the residual gravity values after removing merely the reference gravity model DIR_R5, while Figure 15c shows the final residual gravity values from which additionally the RTM reduction (see Figure 15b) is removed. By comparing these two figures, it is completely obvious that the residual gravity values become smooth after removing the RTM reduction. The relative statistics are shown in Table 3: the RMS of RTM reduction is 11.70 mGal, the RMS of gravity residuals from DIR_R5 is already smaller than that of gravity disturbances from γ_{wgs84} , and the RMS of the final gravity residuals with RTM reduction drops even to 15.72 mGal. The quasi-geoid models within the local area are as follows: Figure 16a shows the local quasi-geoid of EIGEN-6C4 (d/o 500), while Figure 16b shows the local quasi-geoid of the point mass model which is combined with RCR technique and RTM reduction. The differences are mainly in the northwest area, where there is lack of airborne gravity data, and at

Table 3

Statistics of g_{RTM} (RTM Reduction), $g - \gamma_{wgs84}$ (Gravity Disturbances From γ_{wgs84}), $g - g_{DIR_R5}$ (Gravity Residuals From DIR_R5), and $g - g_{DIR_R5} - g_{RTM}$ (Final Gravity Residuals) at the Flight Height

	Minimum	Maximum	Mean	RMS
g_{RTM}	-31.42	66.12	0.03	11.70
$g - \gamma_{wgs84}$	-84.47	119.44	27.24	57.33
$g - g_{DIR_R5}$	-100.49	96.79	-0.15	22.39
$g - g_{DIR_R5} - g_{RTM}$	-81.92	57.74	-0.18	15.72

Note. Unit: mGal.

locations near the border of the research region. In other regions, our point mass model may result in a more detailed gravity field information due to the measurements of the mission and the topography effect which is shown in Figure 16c.

Finally, GNSS/leveling points within the local region are used to investigate the quality of the local quasi-geoid. These GNSS/leveling points are from the EUVN_DA project (Kenyeres et al., 2010). There are in total 42 GNSS/leveling points over Italy. But eight of them are outside the research region or at data gap areas. The distances of these points to GEOHALO measurements are larger than 40 km, and they are marked by triangles in Figure 16d. There are eight other GNSS/leveling points which are closer to the measurement tracks than 40 km. These latter are marked as dots in that figure. All other GNSS/leveling points are given by stars. Figure 16d shows the differences between the height anomalies of the GNSS/leveling points and that from our model. The obtained values are obviously larger for the triangle points than for those indicated by dots. That means that estimation of a reliable quasi-geoid with a dedicated spatial resolution in a not so well surveyed area requires line spacing to the measurements less than the quasi-geoid resolution in question (here 40 km). Otherwise, the quasi-geoid there is less accurate. Hence, in the following we analyze statistically the quality of the obtained quasi-geoid twice: (1) by using all GNSS/leveling points except those marked by the triangles (i.e., 34 points) and (2) by using the remaining 26 points after removing the 8 points indicated by dots. Our respective statistics are shown in Table 4. There RMS simply means root-mean-square of the differences between the height anomalies from the GNSS/leveling points and those from the model to be compared. In contrast, STD is standard deviation between the GNSS/leveling height anomalies and the model after subtraction of the difference mean. From the 34 GNSS/leveling points we obtain the following results: First of all, the RMS of the differences between the height anomalies from the GNSS/leveling points and that from the satellite-only model DIR_R5 is reduced by 1.6 cm when applying the RTM reduction due to the high-frequency gravity information represented by the RTM reduction (DIR_R5 minus DIR_R5+RTM). Furthermore, the inclusion of the GEOHALO measurements by means of the point mass modeling (PMM) gives an improvement by 11 cm (DIR_R5+RTM minus DIR_R5+PPM+RTM). Consequently, RTM reduction and airborne gravimetry on board HALO are suitable to improve satellite-only gravity field models. Furthermore, the RMS of the differences between the height anomalies from the GNSS/leveling points and those from the point mass model results (0.551 m and 0.562 m, respectively) is significantly smaller than that from EIGEN-6C4 (d/o 500). On the other hand, the relative STD after reduction of the mean is 0.356 m and 0.313 m, which is larger than 0.201 m as obtained from EIGEN-6C4 (d/o 500). That means that there exists a small bias between EIGEN-6C4 (d/o 500) and our modeling with respect to the mean values of the differences from GNSS/leveling. The reason may be a nonsymmetric slope from north to south in our measurement region. This has been already reported by Kenyeres et al. (2010) in a comparison between EGG08 and the same GNSS/leveling points which we used in our study. Figure 16d shows that there are more GNSS/leveling points of larger differences to the quasi-geoid in the northern part of the GEOHALO area compared to the south. In the northern part the height differences between GNSS/leveling points and our quasi-geoid are relatively large. This may be one of the reasons that the STD of the differences between height anomalies from GNSS/leveling points and those from final modeling results is larger than that derived from EIGEN-6C4 (d/o 500). Therefore, we have also checked the GNSS/leveling differences by using only the 26 points (stars) after discarding those 8 points indicated by dots. From the latter results, the RMS of our final model is 0.414 m, which is smaller than 0.573 m for EIGEN-6C4 (d/o 500) and both STD are similar (0.225 m and 0.200 m, respectively). Comparing the results using either 34 or 26 GNSS/leveling points, it shows that the statistics for EIGEN-6C4 (d/o 500), DIR_R5, and DIR_R5 with RTM

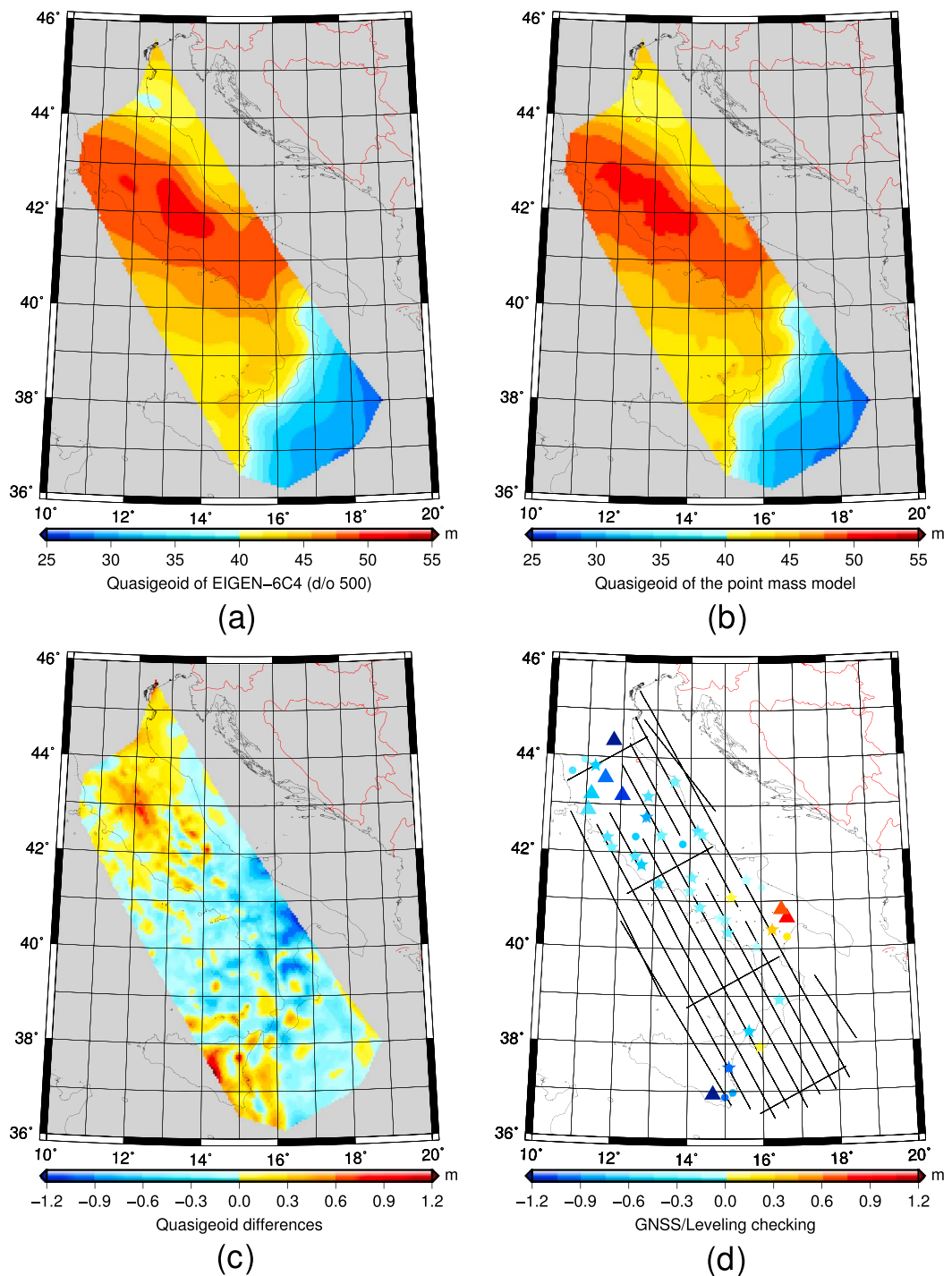


Figure 16. (a) Quasi-geoid derived from the model EIGEN-6C4 up to $N_{\max} = 500$, (b) quasi-geoid derived from the point mass model (183 masses), which is combined with the RCR technology and RTM reduction, (c) quasi-geoid differences, and (d) difference between GNSS/leveling points and the quasi-geoid derived from the point mass model.

reduction are almost the same, but our quasi-geoid results are better when using 26 GNSS/leveling points. Hence, it can be concluded that data gaps in measurements and the border effect have negative influences on quasi-geoid modeling. Apart from that, such measurements from GEOHALO can not only fill in gaps of satellite gravimetry but also improve the local quasi-geoid where only satellite gravimetry data exist. In addition, the quality of a local quasi-geoid can be improved by RTM reduction.

Table 4

Comparison of GNSS/leveling With Different Gravity Field Models (34/26 Points Close to the GEOHALO Measurement Tracks Within the Surveyed Area)

	Minimum	Maximum	Mean	RMS	STD
EIGEN-6C4(d/o 500)	-0.934/-0.934	-0.013/-0.013	-0.579/-0.539	0.612/0.573	0.201/0.200
DIR_R5	-1.400/-1.400	0.702/0.628	-0.500/-0.518	0.688/0.651	0.480/0.402
DIR_R5+RTM	-1.330/-1.330	0.478/0.271	-0.545/-0.568	0.672/0.649	0.398/0.321
DIR_R5+PMM	-1.467/-0.670	0.358/0.358	-0.435/-0.301	0.551/0.404	0.356/0.276
DIR_R5+PMM+RTM	-1.357/-0.625	0.082/0.082	-0.470/-0.350	0.562/0.414	0.313/0.225

Note. Unit: meters. The 34 points are those marked by dots (8 points) and stars (26 points) in Figure 16d.

5. Discussion and Conclusions

The airborne gravimetry of the GEOHALO project is investigated from the basic processing of the gravimetry measurements to final geodetic applications. There are three crucial findings related to the processing of the gravimetry measurements: First, the vertical kinematic accelerations of the jet aircraft calculated from Doppler observations derived from carrier phase measurements are generally better than those from raw Doppler observations. Second, the gravimetry equipment Chekan-AM worked well on the jet aircraft on a high altitude and at high speed according to the two repeat tracks. This helps us to design future airborne gravity campaigns. Last, the RMS of differences at crossover points is 1.4 mGal. This implies (according to the law of error propagation) that the accuracy for our GEOHALO airborne gravimetry is of $1.4/\sqrt{2} \approx 1$ mGal along the tracks. This is more accurate than the gravity field model EIGEN-6C4 (d/o 2190) as the RMS of differences between the GEOHALO gravimetry measurements and gravity values derived from this model is 2.88 mGal (L1(1 Hz)). Regarding geodetic applications, gravity disturbances on the ellipsoid of the point mass model show good agreement with EIGEN-6C4 (d/o 500) at locations of existing measurements. That means that the Chekan-AM instrumentation on board the HALO jet aircraft can help to improve current satellite-only gravity field models, especially in regions with sparse terrestrial data coverage. Furthermore, according to GNSS/leveling comparison, the local quasi-geoid calculated from the GEOHALO measurements is more accurate than the one derived from the satellite-only gravity field model DIR_R5 and reaches the accuracy of EIGEN-6C4 (up to d/o 500) when the topography effect is taken into account. Concluding, the GEOHALO mission was a very successful airborne gravity campaign, which was also an experiment for preparing future campaigns, for instance, in Antarctica.

References

- Barthelmes, F. (1986). *Untersuchungen zur Approximation des äußeren Gravitationsfeldes der Erde durch Punktmassen mit optimierten Positionen*. Veröffentlichungen des Zentralinstituts für Physik der Erde 92. Zentralinstitut für Physik der Erde. Potsdam: Akademie der Wissenschaften der DDR.
- Barthelmes, F. (1988). Local gravity field approximation by point masses with optimized positions. In *Proc. 6th international symposium "Geodesy and Physics of the Earth"*, Potsdam.
- Barthelmes, F., & Dietrich, R. (1991). Use of point masses on optimized positions for the approximation of the gravity field, *Determination of the geoid* (pp. 484–493). New York: Springer.
- Barzaghi, R., Albertella, A., Carrion, D., Barthelmes, F., Petrovic, S., & Scheinert, M. (2016). Testing airborne gravity data in the large-scale area of Italy and adjacent seas. In S. Jin, & R. Barzaghi (Eds.), *IGFS 2014: Proceedings of the 3rd International Gravity Field Service (IGFS)* (pp. 39–44). Shanghai, China: Springer. https://doi.org/10.1007/1345_2015_45
- Blazhnov, B. (2002). Integrated mobile gravimetric system—Development and test results. In *9th Saint Petersburg International Conference on Integrated Navigation Systems*, St. Petersburg (pp. 223–232).
- Borio, D., Sokolova, N., & Lachapelle, G. (2009). Doppler measurements and velocity estimation: A theoretical framework with software receiver implementation. In *Proceedings of the 22nd International Technical Meeting of The Satellite Division of the Institute of Navigation (ION GNSS 2009)*, Savannah, GA (pp. 304–316).
- Bruinsma, S. L., Förste, C., Abrilovskiy, O., Lemoine, J. M., Marty, J. C., Mulet, S., ... Bonvalot, S. (2014). ESA's satellite-only gravity field model via the direct approach based on all GOCE data. *Geophysical Research Letters*, 41, 7508–7514.
- Bruton, A., Glennie, C., & Schwarz, K. (1999). Differentiation for high-precision GPS velocity and acceleration determination. *GPS solutions*, 2(4), 7–21.
- Cannon, M. E., Lachapelle, G., Szarmes, M. C., Hebert, J. M., Keith, J., & Jokerst, S. (1997). DGPS kinematic carrier phase signal simulation analysis for precise velocity and position determination. *Navigation*, 44(2), 231–245.
- Childers, V. A., Bell, R. E., & Brozena, J. M. (1999). Airborne gravimetry: An investigation of filtering. *Geophysics*, 64(1), 61–69.
- Claessens, S., Featherstone, W., & Barthelmes, F. (2001). Experiences with point-mass gravity field modelling in the Perth region, Western Australia. *Geomatics Research Australasia*, 75, 53–86.
- Cooley, J. W., & Tukey, J. W. (1965). An algorithm for the machine calculation of complex Fourier series. *Mathematics of Computation*, 19(90), 297–301.
- Dahl, O., & Forsberg, R. (1998). Geoid models around Sognefjord using depth data. *Journal of Geodesy*, 72(9), 547–556.
- Denker, H. (2013). Regional gravity field modeling: Theory and practical results. In Xu G. (Ed.), *Sciences of Geodesy - II*. Berlin: Springer.

Acknowledgments

The authors thank Editor Paul Tregoning and two anonymous reviewers for their beneficial suggestions and comments, which are of great value for improving the manuscript. The realization of the GEOHALO mission and the investigations based on the acquired data were supported by the German Science Foundation (Deutsche Forschungsgemeinschaft, DFG) in the framework of its Priority Program 1294 "Atmospheric and Earth System Research with the High Altitude and Long Range Research Aircraft (HALO)" by the grants SCHE 1426/5, KU 1207/8, SCHE 1426/9, GE 1911/3, SCHE 1426/17, and FO 771/8. This particular study was supported by the Chinese Scholarship Council (201506270158), the Key Laboratory of Geospace Environment and Geodesy, Ministry Education, Wuhan University (15-01-03 and 16-02-07), the Natural Science Foundation of China (41374023, 41474019, 41504013, and 41604027), and the Shandong Provincial Natural Science Foundation (ZR2016DQ01). Furthermore, the authors would like to express their appreciation to Boyang Zhou of Guangdong University of Technology (GDUT) and Yihao Wu of Huazhong University of Science and Technology (HUST) for their kind help and discussions about the topography effect. Many thanks also to the GEOHALO team especially to Mirko Scheinert from Technical University of Dresden as head of the GEOHALO project. The best airborne gravimetry data from the GEOHALO project presented in this paper are available from GFZ Data Services: <https://doi.org/10.5880/GFZ.1.2.2017.001> and other original data are available on request and can be provided by the corresponding authors by e-mail.

- Forsberg, R. (1984). A study of terrain reductions, density anomalies and geophysical inversion methods in gravity field modelling (Tech. Rep. No. OSU/DGSS-355): Ohio State Univ Columbus Dept Of Geodetic Science And Surveying.
- Förste, C., Bruinsma, S., Abrikosov, O., Lemoine, J. M., Marty, J. C., Flechtner F., ... Biancale R. (2014). EIGEN-6C4—The latest combined global gravity field model including GOCE data up to degree and order 2190 of GFZ Potsdam and GRGS Toulouse, GFZ Data Services. <https://doi.org/10.5880/icgem.2015.1>
- Hardy, R. L., & Göpfert, W. M. (1975). Least squares prediction of gravity anomalies, geoidal undulations, and deflections of the vertical with multiquadric harmonic functions. *Geophysical Research Letters*, 2(10), 423–426.
- Harlan, R. B. (1968). Eotvos corrections for airborne gravimetry. *Journal of Geophysical Research*, 73(14), 4675–4679.
- He, K. (2015). GNSS kinematic position and velocity determination for airborne gravimetry (PhD thesis), Berlin, Technische Universität Berlin, Diss.
- He, K., Xu, G., Xu, T., & Flechtner, F. (2016). GNSS navigation and positioning for the GEOHALO experiment in Italy. *GPS Solutions*, 20(2), 215–224.
- Heck, B., & Seitz, K. (2007). A comparison of the tesseroid, prism and point-mass approaches for mass reductions in gravity field modelling. *Journal of Geodesy*, 81(2), 121–136.
- Hirt, C. (2012). Efficient and accurate high-degree spherical harmonic synthesis of gravity field functionals at the Earth's surface using the gradient approach. *Journal of Geodesy*, 86(9), 729–744.
- Hirt, C. (2013). RTM gravity forward-modeling using topography/bathymetry data to improve high-degree global geopotential models in the coastal zone. *Marine Geodesy*, 36(2), 183–202.
- Jekeli, C. (2001). *Inertial navigation systems with geodetic applications*. Berlin; New York: Walter de Gruyter.
- Kenyeres, A., Sacher M., Ihde J., Denker H., & Marti U. (2010). EUVN_DA: Realization of the European continental GPS/leveling network. In Mertikas, S. P. (Ed.), *Gravity, geoid and Earth observation: IAG Commission 2: Gravity field, Chania, Crete, Greece, 23–27 (pp. 315–320)*. Berlin, Heidelberg: Springer. https://doi.org/DOI: 10.1007/978-3-642-10634-7_41
- Klees, R., Tenzer, R., Prutkin, I., & Wittwer, T. (2008). A data-driven approach to local gravity field modelling using spherical radial basis functions. *Journal of Geodesy*, 82(8), 457–471.
- Krasnov, A., & Sokolov, A. (2015). A modern software system of a mobile Chekan-AM gravimeter. *Gyroscopy and Navigation*, 6(4), 278–287.
- Krasnov, A., Sokolov, A., & Usov, S. (2011). Modern equipment and methods for gravity investigation in hard-to-reach regions. *Gyroscopy and Navigation*, 2(3), 178–183.
- Krasnov, A., Sokolov, A., & Elinson, L. (2014). Operational experience with the Chekan-AM gravimeters. *Gyroscopy and Navigation*, 5(3), 181–185.
- Lu, B., Barthelmes, F., Petrovic, S., Pflug, H., Förste, C., Flechtner, F., ... Scheinert, M. (2017). Airborne Gravimetry Data from GEOHALO project – (Data Set). GFZ Data Services. <https://doi.org/10.5880/GFZ.1.2.2017.001>
- Lu, B., Luo, Z., Zhong, B., Zhou, H., Flechtner, F., Förste, C., ... Zhou, R. (2017). The gravity field model IGGT_R1 based on the second invariant of the GOCE gravitational gradient tensor. *Journal of Geodesy*, 1–12. <https://doi.org/10.1007/s00190-017-1089-8>
- LaCoste, L. J. (1967). Measurement of gravity at sea and in the air. *Reviews of geophysics*, 5(4), 477–526.
- Newton, I., Bernoulli, D., MacLaurin, C., & Euler, L. (1833). *Philosophiae Naturalis Principia Mathematica, Vol 1.*: Excidit G. Brookman; Impensis TT et J. Tegg Londini.
- Pail, R., Bruinsma, S., Migliaccio, F., Förste, C., Goiginger, H., Schuh, W. D., ... Carl, C. T. (2011). First GOCE gravity field models derived by three different approaches. *Journal of Geodesy*, 85(11), 819–843.
- Petrovic, S., Barthelmes, F., & Pflug, H. (2016). Airborne and shipborne gravimetry at GFZ with emphasis on the GEOHALO project. In Rizos, C., & Willis, P. (Eds.), *IAG 150 years: Proceedings of the 2013 IAG Scientific Assembly* (pp. 313–322). Potsdam, Germany: Springer. https://doi.org/10.1007/1345_2015_17
- Rudolph, S., Kusche, J., & Ilk, K. H. (2002). Investigations on the polar gap problem in ESA's gravity field and steady-state ocean circulation explorer mission (GOCE). *Journal of Geodynamics*, 33(1), 65–74.
- Rummel, R., Rapp, R. H., Suenkel, H., & Tscherning, C. C. (1988). Comparisons of global topographic/isostatic models to the Earth's observed gravity field (Tech. Rep. 388, pp. 43210–1247). Columbus, Ohio: The Ohio State University.
- Scheinert, M. (2013). The geodetic-geophysical flight mission GEOHALO to acquire measurements of the gravity and magnetic fields, of GNSS remote sensing and of laser altimetry over the Mediterranean. *EGU General Assembly 2013, held 7-12 April, 2013 in Vienna, Austria*, id. EGU2013-5160.
- Semmling, A., Beckheinrich, J., Wickert, J., Beyerle, G., Schön, S., Fabra, F., ... Scheinert, M. (2014). Sea surface topography retrieved from GNSS reflectometry phase data of the GEOHALO flight mission. *Geophysical Research Letters*, 41, 954–960. <https://doi.org/10.1002/2013GL058725>
- Serrano, L., Kim, D., & Langley, R. B. (2004). A single GPS receiver as a real-time, accurate velocity and acceleration sensor. In *Proceedings of the 17th International Technical Meeting of the Satellite Division of The Institute of Navigation (ION GNSS 2004)* (pp. 2021–2034), Long Beach, CA.
- Sokolov, A. (2011). High accuracy airborne gravity measurements. Methods and equipment. *IFAC Proceedings Volumes*, 44(1), 1889–1891.
- Swain, C. J. (1996). Horizontal acceleration corrections in airborne gravimetry. *Geophysics*, 61(1), 273–276.
- Szarmes, M., Ryan, S., Lachapelle, G., & Fenton, P. (1997). DGPS high accuracy aircraft velocity determination using Doppler measurements. In *Proceedings of the International Symposium on Kinematic Systems (KIS97)*, Banff Alberta Canada (pp. 167–174).
- Wittwer, T. (2009). Regional gravity field modeling with radial basis functions. PhD thesis, NCG, Nederlandse Commissie voor Geodesie, Netherlands Geodetic Commission, Publications on Geodesy 72.
- Wu, Y., Zhou, H., Zhong, B., & Luo, Z. (2017). Regional gravity field recovery using the GOCE gravity gradient tensor and heterogeneous gravimetry and altimetry data. *Journal of Geophysical Research: Solid Earth*, 122, 6928–6952. <https://doi.org/10.1002/2017JB014196>
- Zheleznyak, L. (2010). The accuracy of measurements by the CHEKAN-AM gravity system at sea. *Izvestiya, Physics of the Solid Earth*, 46(11), 1000–1003.
- Zheleznyak, L., Koneshov, V., Krasnov, A., Sokolov, A., & Elinson, L. (2015). The results of testing the Chekan gravimeter at the Leningrad gravimetric testing area. *Izvestiya, Physics of the Solid Earth*, 51(2), 315–320.